Tuning the nonlinear optical absorption of reduced graphene oxide by chemical reduction

Hongfei Shi,[1] Can Wang,[1,*] Zhipei Sun,[2] Yueliang Zhou,[1] Kuijuan Jin,[1,3,5] Simon A. T. Redfern,[4] and Guozhen Yang[1,3]

[1]*Beijing National Laboratory for Condensed Matter Physics, Institute of Physics, Chinese Academy of Sciences, PO Box 603, Beijing 100190, China*
[2]*Department of Micro- and Nanosciences, Aalto University, PO Box 13500, FI-00076 Aalto, Finland*
[3]*Collaborative Innovation Center of Quantum Matter, Beijing, China*
[4]*Department of Earth Sciences, University of Cambridge, Downing Street, Cambridge, CB2 3EQ, UK*
[5]*kjjin@iphy.ac.cn*
**canwang@iphy.ac.cn*

Abstract: Reduced graphene oxides with varying degrees of reduction have been produced by hydrazine reduction of graphene oxide. The linear and nonlinear optical properties of both graphene oxide as well as the reduced graphene oxides have been measured by single beam *Z-scan* measurement in the picosecond region. The results reveal both saturable absorption and two-photon absorption, strongly dependent on the intensity of the pump pulse: saturable absorption occurs at lower pump pulse intensity (~1.5 GW/cm^2 saturation intensity) whereas two-photon absorption dominates at higher intensities (≥5.7 GW/cm^2). Intriguingly, we find that the two-photon absorption coefficient (from 1.5 cm/GW to 4.5cm/GW) and the saturation intensity (from 1 GW/cm^2 to 2 GW/cm^2) vary with chemical reduction, which is ascribed to the varying concentrations of sp^2 domains and sp^2 clusters in the reduced graphene oxides. Our results not only provide an insight into the evolution of the nonlinear optical coefficient in reduced graphene oxide, but also suggest that chemical engineering techniques may usefully be applied to tune the nonlinear optical properties of various nano-materials, including atomically thick graphene sheets.

©2014 Optical Society of America

OCIS codes: (190.0190) Nonlinear optics; (190.4710) Optical nonlinearities in organic materials; (160.0160) Materials; (160.4236) Nanomaterials.

Reference and links

1. F. Bonaccorso, Z. Sun, T. Hasan, and A. C. Ferrari, "Graphene photonics and optoelectronics," Nat. Photonics **4**(9), 611–622 (2010).
2. R. R. Nair, P. Blake, A. N. Grigorenko, K. S. Novoselov, T. J. Booth, T. Stauber, N. M. R. Peres, and A. K. Geim, "Fine structure constant defines visual transparency of graphene," Science **320**(5881), 1308 (2008).
3. K. F. Mak, M. Y. Sfeir, Y. Wu, C. H. Lui, J. A. Misewich, and T. F. Heinz, "Measurement of the optical conductivity of graphene," Phys. Rev. Lett. **101**(19), 196405 (2008).
4. M. Breusing, C. Ropers, and T. Elsaesser, "Ultrafast carrier dynamics in graphite," Phys. Rev. Lett. **102**(8), 086809 (2009).
5. Z. P. Sun, T. Hasan, F. Torrisi, D. Popa, G. Privitera, F. Q. Wang, F. Bonaccorso, D. M. Basko, and A. C. Ferrari, "Graphene mode-locked ultrafast laser," ACS Nano **4**(2), 803–810 (2010).
6. Z. P. Sun, D. Popa, T. Hasan, F. Torrisi, F. Q. Wang, E. J. R. Kelleher, J. C. Travers, V. Nicolosi, and A. C. Ferrari, "A stable, wideband tunable, near transform-limited, graphene-mode-locked, ultrafast laser," Nano Res. **3**(9), 653–660 (2010).
7. T. Hasan, Z. P. Sun, F. Q. Wang, F. Bonaccorso, P. H. Tan, A. G. Rozhin, and A. C. Ferrari, "Nanotube-polymer composites for ultrafast photonics," Adv. Mater. **21**(38â€“39), 3874–3899 (2009).
8. A. Martinez and Z. P. Sun, "Nanotube and graphene saturable absorbers for fibre lasers," Nat. Photonics **7**(11), 842–845 (2013).
9. Z. Sun, T. Hasan, and A. C. Ferrari, "Ultrafast lasers mode-locked by nanotubes and graphene," Physica E **44**(6), 1082–1091 (2012).

#212097 - $15.00 USD Received 14 May 2014; revised 3 Jul 2014; accepted 7 Jul 2014; published 4 Aug 2014
(C) 2014 OSA

10. E. Hendry, P. J. Hale, J. Moger, A. K. Savchenko, and S. A. Mikhailov, "Coherent nonlinear optical response of graphene," Phys. Rev. Lett. **105**(9), 097401 (2010).
11. A. Y. Bykov, T. V. Murzina, M. G. Rybin, and E. D. Obraztsova, "Second harmonic generation in multilayer graphene induced by direct electric current," Phys. Rev. B **85**(12), 121413 (2012).
12. J. J. Dean and H. M. van Driel, "Graphene and few-layer graphite probed by second-harmonic generation: Theory and experiment," Phys. Rev. B **82**(12), 125411 (2010).
13. H. Zhang, S. Virally, Q. L. Bao, L. K. Ping, S. Massar, N. Godbout, and P. Kockaert, "Z-scan measurement of the nonlinear refractive index of graphene," Opt. Lett. **37**(11), 1856–1858 (2012).
14. X. L. Zhang, Z. B. Liu, X. C. Li, Q. Ma, X. D. Chen, J. G. Tian, Y. F. Xu, and Y. S. Chen, "Transient thermal effect, nonlinear refraction and nonlinear absorption properties of graphene oxide sheets in dispersion," Opt. Express **21**(6), 7511–7520 (2013).
15. H. X. Chang, Z. H. Sun, Q. H. Yuan, F. Ding, X. M. Tao, F. Yan, and Z. J. Zheng, "Thin film field-effect phototransistors from bandgap-tunable, solution-processed, few-layer reduced graphene oxide films," Adv. Mater. **22**(43), 4872–4876 (2010).
16. L. Z. Liu, L. Wang, J. F. Gao, J. J. Zhao, X. F. Gao, and Z. F. Chen, "Amorphous structural models for graphene oxides," Carbon **50**(4), 1690–1698 (2012).
17. G. Eda, Y. Y. Lin, C. Mattevi, H. Yamaguchi, H. A. Chen, I. S. Chen, C. W. Chen, and M. Chhowalla, "Blue photoluminescence from chemically derived graphene oxide," Adv. Mater. **22**(4), 505–509 (2010).
18. S. Y. Zhou, G. H. Gweon, A. V. Fedorov, P. N. First, W. A. de Heer, D. H. Lee, F. Guinea, A. H. Castro Neto, and A. Lanzara, "Substrate-induced bandgap opening in epitaxial graphene," Nat. Mater. **6**(10), 770–775 (2007).
19. Y. B. Zhang, T. T. Tang, C. Girit, Z. Hao, M. C. Martin, A. Zettl, M. F. Crommie, Y. R. Shen, and F. Wang, "Direct observation of a widely tunable bandgap in bilayer graphene," Nature **459**(7248), 820–823 (2009).
20. S. F. Pei and H. M. Cheng, "The reduction of graphene oxide," Carbon **50**(9), 3210–3228 (2012).
21. K. P. Loh, Q. Bao, G. Eda, and M. Chhowalla, "Graphene oxide as a chemically tunable platform for optical applications," Nat. Chem. **2**(12), 1015–1024 (2010).
22. Z. B. Liu, Y. Wang, X. L. Zhang, Y. F. Xu, Y. S. Chen, and J. G. Tian, "Nonlinear optical properties of graphene oxide in nanosecond and picosecond regimes," Appl. Phys. Lett. **94**(2), 021902 (2009).
23. X. L. Zhang, X. Zhao, Z. B. Liu, S. Shi, W. Y. Zhou, J. G. Tian, Y. F. Xu, and Y. S. Chen, "Nonlinear optical and optical limiting properties of graphene oxide-fe3o4 hybrid material," J. Opt. **13**(7), 075202 (2011).
24. C. Gómez-Navarro, R. T. Weitz, A. M. Bittner, M. Scolari, A. Mews, M. Burghard, and K. Kern, "Electronic transport properties of individual chemically reduced graphene oxide sheets," Nano Lett. **7**(11), 3499–3503 (2007).
25. T. Remyamol, H. John, and P. Gopinath, "Synthesis and nonlinear optical properties of reduced graphene oxide covalently functionalized with polyaniline," Carbon **59**, 308–314 (2013).
26. X. F. Jiang, L. Polavarapu, S. T. Neo, T. Venkatesan, and Q. H. Xu, "Graphene oxides as tunable broadband nonlinear optical materials for femtosecond laser pulses," J. Phys. Chem. Lett. **3**(6), 785–790 (2012).
27. Z.-B. Liu, X. Zhao, X.-L. Zhang, X.-Q. Yan, Y.-P. Wu, Y.-S. Chen, and J.-G. Tian, "Ultrafast dynamics and nonlinear optical responses from sp2- and sp3-hybridized domains in graphene oxide," J. Phys. Chem. Lett. **2**(16), 1972–1977 (2011).
28. S. Park, J. H. An, I. W. Jung, R. D. Piner, S. J. An, X. S. Li, A. Velamakanni, and R. S. Ruoff, "Colloidal suspensions of highly reduced graphene oxide in a wide variety of organic solvents," Nano Lett. **9**(4), 1593–1597 (2009).
29. F. Bonaccorso, A. Lombardo, T. Hasan, Z. P. Sun, L. Colombo, and A. C. Ferrari, "Production and processing of graphene and 2d crystals," Mater. Today **15**(12), 564–589 (2012).
30. F. Bonaccorso and Z. P. Sun, "Solution processing of graphene, topological insulators and other 2d crystals for ultrafast photonics," Opt. Mater. Express **4**(1), 63–78 (2014).
31. M. Sheikbahae, A. A. Said, T. H. Wei, D. J. Hagan, and E. W. Vanstryland, "Sensitive measurement of optical nonlinearities using a single beam," IEEE J. Quantum Electron. **26**(4), 760–769 (1990).
32. S. Yumitori, "Correlation of c1s chemical state intensities with the o1s intensity in the xps analysis of anodically oxidized glass-like carbon samples," J. Mater. Sci. **35**(1), 139–146 (2000).
33. R. J. Waltman, J. Pacansky, and C. W. Bates, "X-ray photoelectron spectroscopic studies on organic photoconductors evaluation of atomic charges on chlorodiane blue and p(diethylamino)benzaldehyde diphenylhydrazone," Chem. Mater. **5**(12), 1799–1804 (1993).
34. A. C. Ferrari and J. Robertson, "Interpretation of raman spectra of disordered and amorphous carbon," Phys. Rev. B **61**(20), 14095–14107 (2000).
35. Y. Shen, P. Zhou, Q. Q. Sun, L. Wan, J. Li, L. Y. Chen, D. W. Zhang, and X. B. Wang, "Optical investigation of reduced graphene oxide by spectroscopic ellipsometry and the band-gap tuning," Appl. Phys. Lett. **99**(14), 141911 (2011).
36. S. Saxena, T. A. Tyson, S. Shukla, E. Negusse, H. Y. Chen, and J. M. Bai, "Investigation of structural and electronic properties of graphene oxide," Appl. Phys. Lett. **99**(1), 013104 (2011).
37. V. H. Pham, T. V. Cuong, T. D. Nguyen-Phan, H. D. Pham, E. J. Kim, S. H. Hur, E. W. Shin, S. Kim, and J. S. Chung, "One-step synthesis of superior dispersion of chemically converted graphene in organic solvents," Chem. Commun. (Camb.) **46**(24), 4375–4377 (2010).
38. D. I. Kovsh, S. Yang, D. J. Hagan, and E. W. Van Stryland, "Nonlinear optical beam propagation for optical limiting," Appl. Opt. **38**(24), 5168–5180 (1999).

#212097 - $15.00 USD Received 14 May 2014; revised 3 Jul 2014; accepted 7 Jul 2014; published 4 Aug 2014
(C) 2014 OSA

39. R. L. Sutherland, *Handbook of Nonlinear Optics* (Marcel Dekker, 1996).
40. J. Robertson and E. P. O'Reilly, "Electronic and atomic structure of amorphous carbon," Phys. Rev. B Condens. Matter **35**(6), 2946–2957 (1987).

1. Introduction

Graphene has attracted widespread interest due to its unique linear and nonlinear optical properties [1]. Broadband universal absorption [2,3], ultrafast carrier dynamics [4] and band-filling effects [5,6] make it a promising broadband fast-saturable absorber for various applications, including ultrafast lasers [7–9]. The high nonlinear susceptibility of graphene can also potentially enable high-efficiency optical frequency conversion (e.g., four wave mixing [10], harmonic generation [11,12] and nonlinear refraction [13,14]).

An important related material in the graphene family, graphene oxide (GO), also possesses obvious nonlinear optical properties. GO can be thought of as pristine graphene decorated by chemical functionalization [15]. Its electronic band structure can be tuned over a wide range by adjusting the amount and type of oxygen-containing groups [16]. The band gap of GO can vary from 2.2 to 0.5eV [17], which indicates that transitions from insulator to semiconductor and further to semimetal may also be possible [18,19]. In fact, complete reduction of GO can almost restore the physical structure of pristine graphene [20]. The reductive transitions typically lead to changes in electrical transport properties [21]. Recently, the nonlinear optical properties of these two graphene materials (i.e., GO and reduced grapheme oxide, RGO) have attracted much attention, including their two photon absorption (TPA) properties as well as saturable absorption phenomena (SA) [22]. The TPA effect makes GO a promising optical limiter (OL) [23]. The physical structure and properties of RGO lie between GO and pristine graphene. RGO not only exhibits photoluminance [17] like GO, but also field effects [24] like pristine graphene. Note that, in the field of nonlinear optics, although some studies of GO and RGO have been reported [25–27], the mechanisms behind the nonlinear optical properties of RGO are not fully understood. In particular, the evolution of the nonlinear optical properties of RGO on reduction from GO has not been reported thus far.

In this paper, we prepared various RGO (from GO) and GO samples, and demonstrate that RGO can show both SA and TPA effects depending on the pump intensity: SA typically occurs at lower intensity levels (~1.5 GW/cm^2) whereas TPA tends to dominate at higher pump intensity (≥5.7 GW/cm^2). We also find that the TPA coefficient and the saturation intensity increase with reduction, which is related to the sp^2 domains and sp^2 clusters in RGO. We discuss the mechanisms behind the nonlinear optical properties of RGO in the context of our observations, and address the nonlinear property evolution in these atomically thick materials.

2. Sample preparation and characterization methods

The RGO samples were fabricated by hydrazine reduction following the process described previously [28]. In summary, 3 mg GO powder (produced by a modified Hummers method [29,30]) was dispersed in 1 mL deionized water with 40 minutes of sonication. The suspension was diluted by adding 9 mL N,N-Dimethylformamide (DMF) and centrifuged at 3000 rpm for 5 minutes (Anke TDL-60B) to remove any relatively large particles. Hydrazine hydrate was used to reduce GO. After adding hydrazine hydrate, the light-brown suspension was stirred in a water bath at 80 °C for 12 hours. The suspensions with hydrazine turned into black upon reduction, and the concentration of the obtained RGO dispersion was controlled at around 0.3 mg/ml. The degree of reduction, corresponding to the residual number of oxygen-containing groups in RGO, was controlled by adjusting the dose of hydrazine hydrate. Four samples, reduced with 0 μl, 0.45 μl, 1 μl, and 4 μl hydrazine (noted as GO, RGO0.45, RGO1, RGO4 respectively in the following parts of this paper), were used for this investigation. The

#212097 - $15.00 USD Received 14 May 2014; revised 3 Jul 2014; accepted 7 Jul 2014; published 4 Aug 2014
(C) 2014 OSA

dispersion samples are illustrated in Fig. 1, and remain uniform, in a stable colloidal state, for months.

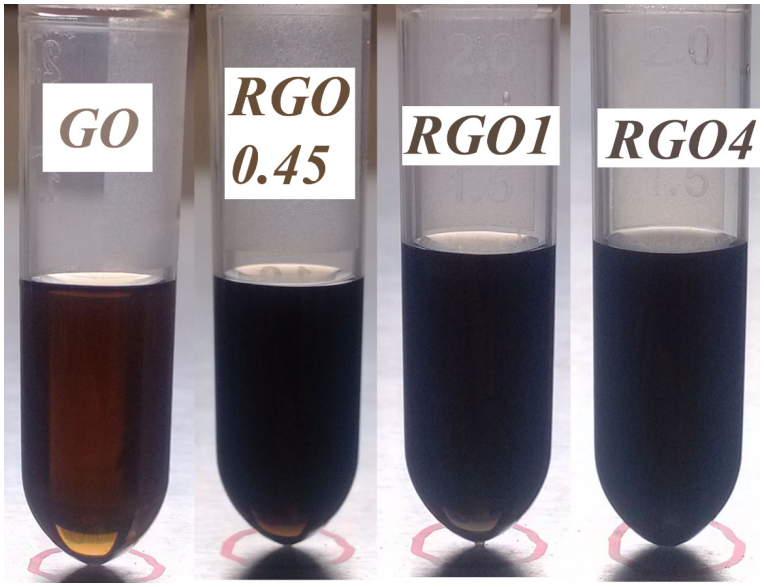

Fig. 1. The GO and RGO dispersions used in this study.

The as-synthesized dispersion samples were characterized by X-ray photoelectron spectroscopy (XPS, ESCALAB 250), UV-vis spectroscopy (SpectraPro-500i) and Raman spectroscopy (JY-T64000) to determine their fundamental physical and chemical properties. For XPS and Raman measurements, the dispersion samples were drop-cast onto Si_3N_4/Si substrates and dried at 50 °C in a vacuum oven. In addition, samples were spray-coated onto quartz substrates pre-heated to 50 °C and subsequently dried at 50 °C in a vacuum oven prior to measuring UV-vis spectroscopy. A similar quantity of sample (~2 ml) was used in each case to get similar film thicknesses for comparative purposes. The single beam Z-scan method was employed to measure the optical nonlinearity of the dispersion samples, using a 532 nm Nd: YAG laser with 25 ps (τ) pulse duration and 1 Hz repetition rate. The laser output was focused using an f = 200 mm lens, giving about ~2.5 mm Rayleigh length (z0) and ~20.6 μm beam waist (ω_0). A range of dispersions (GO, RGO0.45, RGO1, and RGO4) were held within 1 mm thick quartz cells for nonlinear optical measurement. The cell is fixed perpendicular to the laser beam and moved along the optical axis on a linear displacement platform [31]. The transmitted laser light was collected by a large-aperture lens (up to 40 mm) for accurate measurement. To calibrate this measurement setup, a standard CS_2 liquid sample in an identical 1 mm quartz cell is also measured with a laser intensity of 2.7 GW/cm^2. The Reχ^3 of our CS_2 sample in this configuration was -2.9×10^{-12} esu, comparable to that reported for CS_2 [31], validating the accuracy of our measurement setup and analysis methods.

3. Results and discussion

3.1. XPS, Raman and linear absorption

XPS spectra of GO and RGO samples are reported in Fig. 2. The C-C binding energy was assigned at around 284.7 eV. Chemical shifts of + 1.5, + 2.5, + 4.0 eV were used for functional groups C-OH, C = O, and O = C-OH respectively [32]. In the RGO samples, a new sub-peak at 285.8 eV appears, corresponding to the C within the C-N bonds of hydrazones [33]. XPS spectra have been fitted with sub-peaks corresponding to the functional groups.

#212097 - $15.00 USD Received 14 May 2014; revised 3 Jul 2014; accepted 7 Jul 2014; published 4 Aug 2014
(C) 2014 OSA

The percentage area of each sub-peak and the calculated C/O ratio for the four samples are listed in Table 1. As might be expected, oxygen containing groups in RGO are removed gradually, to an increasing degree as larger doses of hydrazine hydrate are used. The maximum C/O ratio of the RGO in this study is around 3.2. Note that increasing the dose of hydrazine to greater that 4 μL did not increase the C/O ratio further, indicating a moderate further influence on the reduction of GO at these levels.

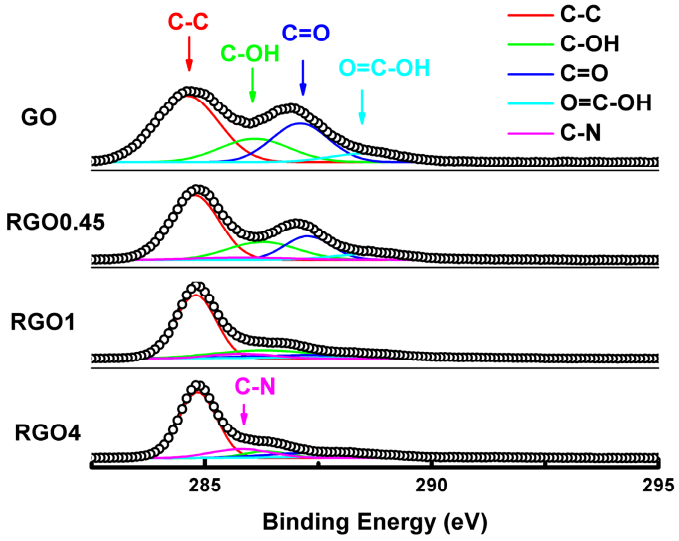

Fig. 2. XPS spectra of samples GO, RGO0.45, RGO1, and RGO4. Peaks are (1) C-C, (2)C-N, (3)C-OH, (4)C = O, (5)O = C-OH.

Table 1. Characteristics of our four samples. The chemical bond and element composition have been obtained from XPS spectra. Oxygen-containing groups are partially removed while C-N bonds arise after reduction. The D/G band ratios (I_D/I_G) and π-π* absorption peak positions are measured from Raman and UV-vis absorption spectra respectively. The TPA coefficient (β) and saturation intensity (I_s) obtained from Z-scan experiments are also listed.

parameters	GO	RGO0.45	RGO1	RGO4
C-C	48.31%	51.13%	55.57%	61.75%
C-OH	18.75%	19.76%	19.06%	7.31%
C = O	25.23%	17.40%	10.92%	11.33%
O = C-OH	7.69%	8.02%	7.17%	6.19%
C-N	0%	3.66%	7.26%	13.40%
C/O	1.68	1.87	2.26	3.22
C/N	∞	27.3	13.8	7.5
I_D/I_G	0.88	0.95	1.03	1.12
π-π* absorption peak position (nm)	231	239	250	257
α_0 @ 532 nm (m^{-1})	426.55	880.67	1417.01	1609.12
β(cm/GW)	1.44	2.67	4.47	4.60
I_s (cm^2/GW)	1.5	2	2.3	2.5

Raman spectra of the RGO samples are given in Fig. 3. We focus here on the ratio of intensities of the D band and G band (I_D/I_G), which contains the information on the average sp^2 cluster size or effective in-plane correlation length L_a. An empirical relationship between L_a and I_D/I_G exists, and has been reported as L_a = 44Å/(I_D/I_G) [34]. The I_D/I_G values obtained thus from our Raman spectra of the GO and RGO samples, imply an average sp^2 region

#212097 - $15.00 USD Received 14 May 2014; revised 3 Jul 2014; accepted 7 Jul 2014; published 4 Aug 2014
(C) 2014 OSA

dimension, or effective in-plane correlation length L_a of ~5.0 nm, ~4.6 nm, ~4.2 nm and~3.9 nm for GO, RGO0.45, RGO1 and RGO4 respectively. The result is consistent with previous reports and can be explained by the emergence of small sp^2 domains on reduction [17]. We estimate the average size of sp^2 cluster to be ~5 nm given sp^2 cluster only occur in GO. For RGO, L_a reflects not only the sp^2 cluster size, but also the sp^2 domain size.

Figure 4 shows the normalized linear absorption spectra of our samples. For each curve, there is an absorption peak in UV region, which originates from the π-π* absorption [35]. A red shift is observed for the absorption peak, shifting from 231 nm to 257 nm upon reduction of GO. This shift can be understood in terms of the restored electronic conjugation pulling the highest occupied molecular orbital and lowest unoccupied molecular orbital back toward the unperturbed π-π* position [36]. This phenomenon is consistent with previous reports [37].

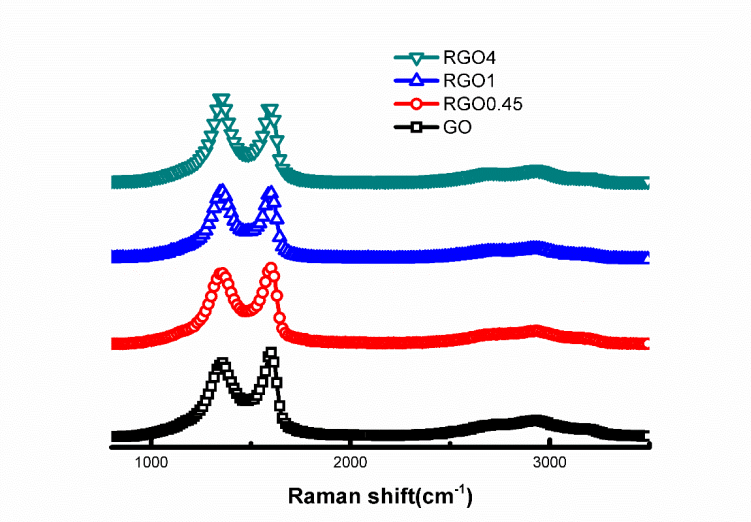

Fig. 3. Raman spectra of the four samples under study. The ratio between D band and G band increases from 0.87 to 1.13 as the degree of reduction increases.

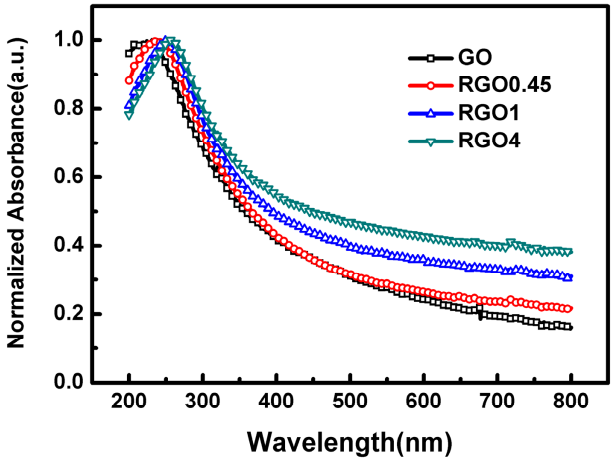

Fig. 4. UV-vis spectrum of spray-coated samples. The main absorption peak shows a redshift from 231 nm to 257 nm upon reduction. All curves are normalized to maximum peak absorbance.

#212097 - $15.00 USD Received 14 May 2014; revised 3 Jul 2014; accepted 7 Jul 2014; published 4 Aug 2014
(C) 2014 OSA

3.2. Open aperture Z-scans

Results from open aperture Z-scan measurements of our RGO and GO dispersion samples are shown in Fig. 5. All samples were measured at four input pulse energies: 0.4 μJ, 0.7 μJ, 1 μJ, and 1.3 μJ. For all samples SA is typically observed at lower pulse energy levels, while higher pump energy leads to TPA.

To better understand our Z-scan measurement results, we consider TPA and SA simultaneously [22]. We use the beam propagation expression from Maxwell's equations to describe the propagation of electrical field along the z-axis in the samples. Assuming cylindrical symmetry, the optical electrical field (E) can be expressed as [38]:

$$2jk\frac{\partial E}{\partial z}=\left(\frac{\partial^2}{\partial r^2}+\frac{1}{r}\frac{\partial}{\partial r}+k_0^2\chi_{NL}^{'}(r,z)\right)E \tag{1}$$

where

$$\begin{aligned}\chi_{NL}^{'}(r,z)&=2n_0\Delta n(r,z)-j\,{}^{n_0}\!/_{k_0}\,\alpha\\ \Delta n&=n_2 I\\ \alpha&=\frac{\alpha_0}{1+{}^{I}\!/_{I_s}}+\beta I\end{aligned} \tag{2}$$

and r and z are the space coordinates perpendicular and parallel to the beam propagation direction, respectively. The wave vector in vacuum is k_0 and k is that in medium ($k = n_0*k_0$) where n_0 is the refractive index of the medium. The intensity is $I = 2n_0^2c|E|^2$.

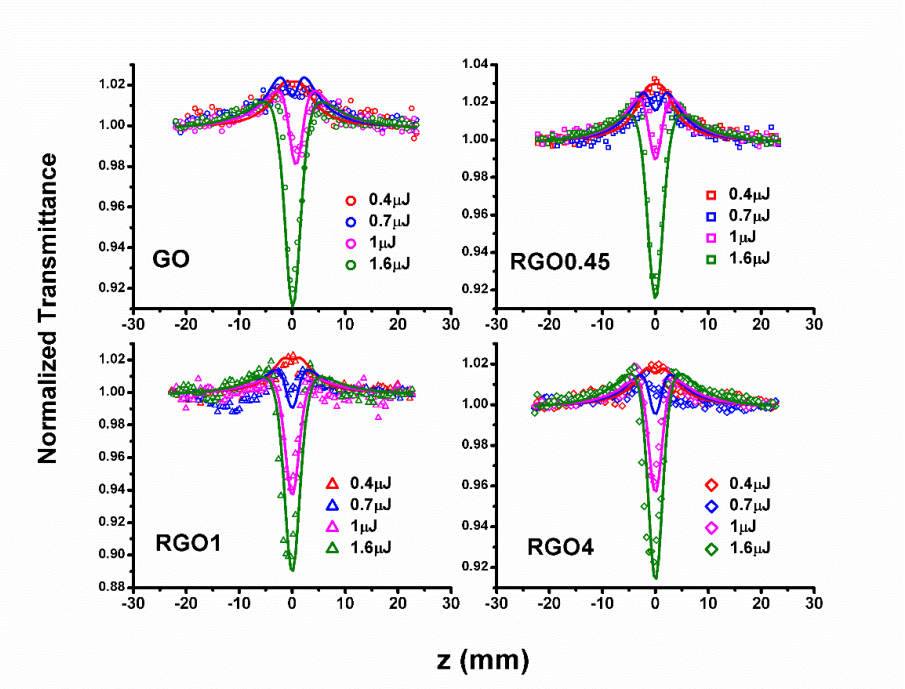

Fig. 5. Open aperture Z-scan curves of GO and RGO samples measured at different pulse energy. The symbols represent experimental data and the solid lines are the results from our simulations.

#212097 - $15.00 USD Received 14 May 2014; revised 3 Jul 2014; accepted 7 Jul 2014; published 4 Aug 2014
(C) 2014 OSA

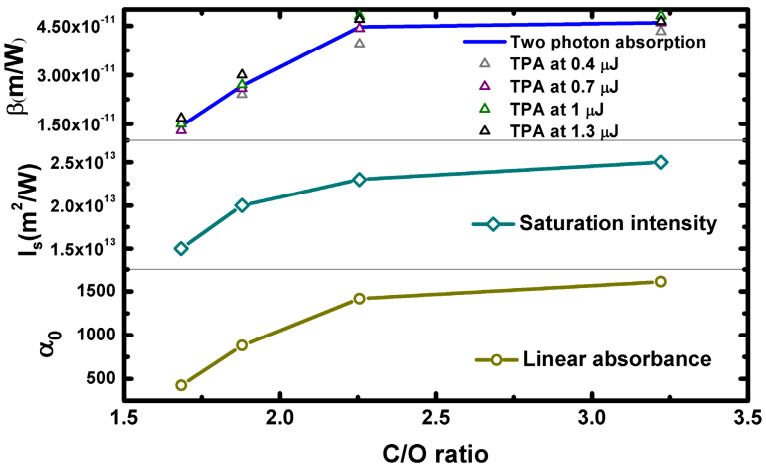

Fig. 6. Linear absorbance, saturation intensiy, and TPA coefficents of the GO and RGO samples as a function of C/O ratio. Open triangles represent TPA coefficents measured at different pulse energy. The average of the data is given by the solid line as a guide to the eye.

Equation (2) demonstrates that four fundamental parameters are typically needed to describe the samples' nonlinear optical properties: the nonlinear refractive index n_2, the linear absorbance α_0, the saturation intensity I_s, and the TPA coefficient β. We also carried out closed-aperture Z-scan measurements. The closed aperture Z-scan curves for all GO and RGO samples that we obtained are very close to that of pure DMF (not shown), which implies that GO or RGO in solution do not significantly contribute to the closed aperture Z-scan results. In other words, n_2 for all our samples can be assumed to be approximately equal to that of the pure DMF, which is determined to be 8.54×10^{-19} m^2/W from the closed aperture Z-scan experiment. The linear absorbance α_0 was calculated from the sample transmittance measured at very low intensity (~0.027 GW/cm^2) at 532 nm. It is well known that β is typically dependent on input pulse energy (i.e., the input pulse intensity) while the saturation intensity I_s can be considered independent of the pump energy [22]. Thus, the above equation can be numerically solved using the Crank-Nicholson finite difference method [38]. The simulation results are plotted in Fig. 5 and show a good match to both the SA and TPA behavior obtained from our experimental results (dots).

The nonlinear absorption coefficients obtained from our analysis are summarized in Fig. 6, and listed in Table 1. Open triangles in Fig. 6 represent β calculated for different pump intensities. We find that β increases slightly as the input pulse energy increases. This implies that, in addition to TPA, excited state absorption from the TPA excited state may also contribute to the nonlinear absorption at higher intensity [14]. This type of excited state absorption, followed by TPA, is particularly attractive for optical limiting applications [39]. As shown in Table 1, the magnitude of I_s and β of our GO are comparable to those previously reported on GO dispersions [14,22]. We also observe that the linear absorbance, saturation intensity and TPA coefficient all increase with reduction, clearly indicating the dependence of RGO nonlinearity on GO reduction. Our result gives a clear insight into the evolution of the nonlinear optical properties of graphene oxide materials with different amount of sp^2 domain, as discussed below.

#212097 - $15.00 USD Received 14 May 2014; revised 3 Jul 2014; accepted 7 Jul 2014; published 4 Aug 2014
(C) 2014 OSA

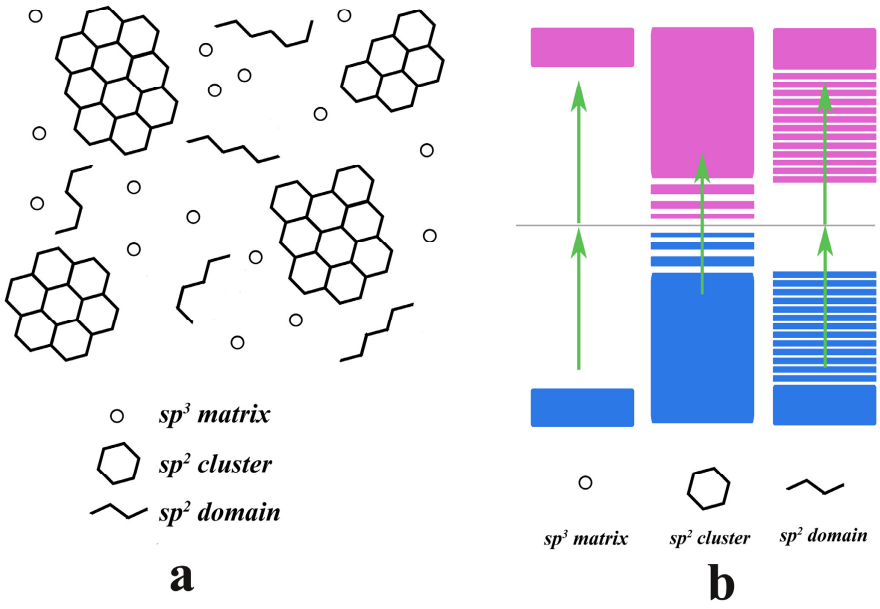

Fig. 7. Structure and band diagram of RGO. The left cartoon (a) illustrates the three regions present in RGO: sp^3 matrix, sp^2 cluster and sp^2 domain. It should be noted that there are no sp^2 domains in GO, but the sp^3 matrix and sp^2 clusters are almost identical to those in RGO. The right hand side (b) illustrates the band gap of the three regions in RGO (pink and blue represent conduction and valence band, respectively). For sp^3 matrix and sp^2 cluster, the band gap are about 6eV and 0.5eV, respectively. The band gap of sp^2 domains varies from 6 eV to 0.5 eV, depending on their size. The photon energy used was 2.3 eV (532 nm). Single and TPA routes are illustrated by green arrows. Single photon absorption exists in sp^2 clusters while two photon absorption exists in the sp^3 matrix. Both single and TPA exist in sp^2 domains.

Our experimental results may be understood on the context of an amorphous structural model for GO and RGO [16]. In this model, oxygen-containing groups tend to aggregate amorphously, forming a sp^3 matrix in which isolated sp^2 cluster islands (size ~5 nm) are buried (Fig. 7). The sp^2 clusters are bunches of well-patterned aromatic rings formed in the oxidation process when originally producing GO from graphite. After reduction, the sp^2 clusters typically do not change, but instead smaller conducting sp^2 domains form and grow within the sp^3 matrix [17]. The sp^2 domains are irregular conjugate carbon bonds, smaller in size than the cluster islands, and produced during reduction. Different regions in the RGO develop different electronic energy structures: the sp^3 matrix typically has an σ-σ* band gap of ~6 eV [40]; the sp^2 clusters normally have a semiconductor band structure with a band gap of ~0.5 eV [17]; while the sp^2 domains' energy (typically from 0.5 to 6 eV) structures depend on their size [17]. The band diagram of these various components of RGO is illustrated in Fig. 7. The photo energy we used (2.26 eV) is well below the sp^3 matrix band gap, but above the sp^2 cluster band gap. The photon energy is likely comparable to the band gap of sp^2 domains. It follows that TPA will mainly arise within the sp^3 matrix, while SA is associated with the sp^2 clusters. Both TPA and SA may be present in the sp^2 domains. Expression for the optical absorption of GO and RGO are, therefore [22,39]:

#212097 - $15.00 USD Received 14 May 2014; revised 3 Jul 2014; accepted 7 Jul 2014; published 4 Aug 2014
(C) 2014 OSA

$$\alpha^{GO}(I)=\frac{N_c\sigma_c^0}{1+I/I_{sc}}+N_m\sigma_m^{TPA}I=\frac{\alpha_0^{GO}}{1+I/I_s^{GO}}+\beta^{GO}I$$
$$\alpha^{RGO}(I)=\frac{N_c\sigma_c^0}{1+I/I_{sc}}+\frac{fN_m\sigma_d^0}{1+I/I_{sd}}+(1-f)N_m\sigma_m^{TPA}I+fN_m\sigma_d^{TPA}I=\frac{\alpha_0^{RGO}}{1+I/I_s^{RGO}}+\beta^{RGO}I \quad (3)$$

We denote the number density of carbon sites in GO's sp^2 clusters (sp^3 matrix) as N_c (N_m) and $N_c + N_m$ corresponds to the total carbon atomic number density. In RGO, the fraction of carbon sites that are converted from the sp^3 matrix to sp^2 domains is f. In the expression for the optical absorption of RGO, the first and second terms represent the SA originating from the sp^2 clusters and sp^2 domains respectively. The linear optical absorption cross section and saturation intensity of sp^2 clusters (with the equivalent values for domains in parentheses) are σ_c^0 (σ_d^0) and I_{sc} (I_{sd}). These terms may be combined into an effective SA term in which α_0^{RGO} and I_s^{RGO} are the effective linear absorbance and saturation intensity. Similarly, the TPA cross section, representing contributions from sp^3 matrix (σ_m^{TPA}) and sp^2 domain (σ_d^{TPA}), may be expressed in terms of a single effective TPA coefficient (β^{RGO}). Larger values of f correspond to increased reduction. Here, we compare the RGO samples (RGO0.45, RGO1, RGO4) with GO to obtain a qualitative comparison of the nonlinear optical properties of sp^2 domains, sp^2 clusters and the sp^3 matrix.

Detailed information about the nonlinear optical properties of these three regions can be derived from Eq. (3) and our experiment results. We consider the TPA first on account of its relative simplicity. For RGO, $\beta^{RGO} = (1-f)\, N_m\, \sigma_m^{TPA} + f\, N_m\, \sigma_d^{TPA} > \beta^{GO} = N_m\, \sigma_m^{TPA}$, which implies that $\sigma_d^{TPA} > \sigma_m^{TPA}$. A carbon site in a sp^2 domain has a larger TPA coefficient than one in the sp^3 matrix. The analysis of SA is more complex. For simplicity, we assume that $I \ll I_{sc}$, I_{sd}, I_s^{GO}, I_s^{RGO} and that the terms of SA in Eq. (3) can be rewritten as:

$$N_c\sigma_c^0\left(1+I/I_{sc}\right)=\alpha_0^{GO}\left(1+I/I_s^{GO}\right)$$
$$N_c\sigma_c^0\left(1+I/I_{sc}\right)+fN_m\sigma_d^0\left(1+I/I_{sd}\right)=\alpha_0^{RGO}\left(1+I/I_s^{RGO}\right) \quad (4)$$

Hence, the linear absorbance and saturation intensities of different regions are:

$$\alpha_0^{GO}=N_c\sigma_c^0$$
$$I_s^{GO}=I_{sc}$$
$$\alpha_0^{RGO}=N_c\sigma_c^0+fN_m\sigma_d^0$$
$$N_c\sigma_c^0\left(1/I_{sc}-1/I_s^{RGO}\right)=fN_m\sigma_d^0\left(1/I_s^{RGO}-1/I_{sd}\right) \quad (5)$$

It can be seen that α_0^{RGO} increases with f, or the reduction degree, which explains the observed increase of linear absorbance with reduction. Since $I_s^{RGO} > I_s^{GO}$, both sides of the final equation are positive, thus $I_{sd} > I_s^{RGO} > I_s^{GO} = I_{sc}$. The saturation intensity of sp^2 domains is larger than that of the sp^2 clusters. The sp^2 domains generated in GO during chemical reduction to RGO thus show both larger saturation intensities and larger TPA cross section.

The TPA in GO and RGO can be dominated by excited state absorption, potentially making GO and RGO good optical limiter materials. In an RGO-based optical limiter, before the pump intensity reaches the level for TPA, the SA effect may relax more energy leading to better transparency, which is somewhat unexpected. If the saturation intensity is pushed beyond the threshold of TPA, then SA will no longer influence the optical limiting process. We also estimate that sp^2 domains have higher I_s than that of the sp^2 clusters, as well as larger TPA cross sections. This implies that producing more sp^2 domains in the samples will favor optical limiting effects and suppress saturation absorption at low working intensities. It is also

#212097 - $15.00 USD Received 14 May 2014; revised 3 Jul 2014; accepted 7 Jul 2014; published 4 Aug 2014
(C) 2014 OSA

worth noting that the contribution of sp^2 domains to both SA and TPA is size-dependent. This suggests that a better saturable absorber or optical limiter can be obtained by tuning the size of sp^2 domains in RGO through chemical engineering.

4. Conclusions

The nonlinear optical absorption properties of RGO and GO are closely related to their microstructures. The three oxidation-reduction related regions in RGO and GO (the sp^3 matrix, sp^2 clusters, and sp^2 domains, respectively) provide different contributions. Any sp^2 domains generated by chemical reduction not only show larger saturation intensities than sp^2 clusters but also larger TPA cross sections than the sp^3 matrix. This relationship may also be applicable to many other carbonaceous materials in which these three regions are commonly found. Our results imply that chemical engineering techniques may usefully be employed to tune the nonlinear optical properties of various nano-materials at atomic-layer thicknesses. For example, by moderate reduction, inducing a greater proportion of sp^2 domains, one could obtain larger TPA in RGO to develop better optical limiters.

Acknowledgments

This work is supported by the National Key Basic Research Program of China (Grant No. 2013CBA01703), the National Natural Science Foundation of China (No. 11174355), Teknologiateollisuus TT-100, the European Union's Seventh Framework Programme (REA grant agreement No. 631610), and Aalto University (Finland).